

This item is the archived peer-reviewed author-version of:

The role of carbon monoxide in the catalytic synthesis of endohedral carbyne

Reference:

Mehmonov Kamoliddin, Ergasheva Aziza, Yusupov Maksudbek, Khalilov Umedjon.- The role of carbon monoxide in the catalytic synthesis of endohedral carbyne

Journal of applied physics / American Institute of Physics - ISSN 1089-7550 - 134:14(2023), 144303

Full text (Publisher's DOI): <https://doi.org/10.1063/5.0160892>

To cite this reference: <https://hdl.handle.net/10067/2012330151162165141>

The Role of Carbon Monoxide in the Catalytic Synthesis of Endohedral Carbyne

Kamoliddin Mehmonov^a, Aziza Ergasheva^a,
Maksudbek Yusupov^{b,c} and Umedjon Khalilov^{d,e,f,*}

^a Arifov Institute of Ion-Plasma and Laser Technologies, Academy of Sciences of Uzbekistan, Tashkent, 100125, Uzbekistan

^b Central Asian University, Tashkent, 111221, Uzbekistan

^c Tashkent International University of Education, Tashkent 100207, Uzbekistan

^d New Uzbekistan University, Tashkent, 100007, Uzbekistan

^e National Research University TIIAME, Tashkent, 100000, Uzbekistan

^f University of Antwerp, Antwerp, 2610, Belgium

* e-mail: umedjon.khalilov@uantwerpen.be (corresponding author)

The unique physical properties of carbyne, a novel carbon nanostructure, have attracted considerable interest in modern nanotechnology. While carbyne synthesis has been accomplished successfully using diverse techniques, the underlying mechanisms governing the carbon monoxide-dependent catalytic synthesis of endohedral carbyne remain poorly understood.

In this simulation-based study, we investigate the synthesis of endohedral carbyne from carbon and carbon monoxide radicals in the presence of a nickel catalyst inside double-walled carbon nanotubes with a (5,5)@(10,10) structure. The outcome of our investigation demonstrates that the incorporation of the carbon atom within the Ni_n@(5,5)@(10,10) model system initiates the formation of an elongated carbon chain. In contrast, upon the introduction of carbon monoxide radicals, the growth of the carbyne chain is inhibited as a result of the oxidation of endohedral nickel clusters by oxygen atoms after the initial steps of nucleation.

Our findings align with prior theoretical, simulation, and experimental investigations, reinforcing their consistency, and providing valuable insights into the synthesis of carbyne-based nanodevices that hold promising potential for future advancements in nanotechnology.

Keywords: *double wall carbon nanotube, nickel catalyst, endohedral carbyne, molecular dynamics, catalytic synthesis, oxygen effect, catalyst poisoning.*

Introduction

Carbon-based nanomaterials, including graphene, carbon nanotubes, and others, hold significant importance in modern nanotechnology [1]. Among them, carbyne, an intriguing 1D sp^1 -hybridized allotrope of carbon [2,3], features a linear chain of carbon atoms connected through alternating single-triple (polyyne) or double-double (cumulene) bonds [4,5], making it a promising material for future nanotechnology [6-8]. In recent years, carbyne has gained extensive attention in experimental studies due to its remarkable physical and chemical properties [4,7-9]. Notably, carbyne exhibits exceptional mechanical strength, surpassing that of graphene, carbon nanotubes, and even diamond by a factor of two [10]. Additionally, carbyne displays high thermal conductivity, reaching 148 kW/m/K [11]. With its compelling attributes, carbyne is considered a promising nanomaterial for various applications, particularly in the fields of microelectronics [12] and hydrogen storage, where its gravimetric storage capacity exceeds 8 wt.% [13].

Carbyne synthesis can be achieved through various growth methods, such as laser ablation [14,15], arc discharge [16-18], electrochemical synthesis [19], on-surface synthesis [20,21], and electron irradiation [22]. However, the synthesis of carbyne or long linear carbon chains (LLCCs) presents significant challenges due to their high reactivity and instability [8,18,23,24]. To address this, researchers have focused on the interior of single-, double-, and multiwalled carbon nanotubes (i.e., SWNTs, DWNTs, and MWNTs, respectively), providing an ideal environment for the synthesis of extended carbyne chains with over a hundred atoms [8,25-27]. In particular, a notable achievement was made by Zhao and colleagues, who reported the first record-long carbon chain containing over 100 carbon atoms within an MWNT using the arc-discharge method [16]. However, the arc-discharge method can only grow LLCC inside MWCNT (i.e., LLCC@MWCNT), and researchers are aiming to achieve LLCC@SWCNT or LLCC@DWCNT by adjusting the growth conditions [8]. Subsequently, Shi et al. achieved the growth of a record-long carbyne chain comprising 6000 carbon atoms inside a DWNT using the heat-treatment method, which remains an unbeaten record to date [25]. Researchers also found that tube structure (chirality) and diameter (curvature) significantly influence the synthesis of confined LLCCs [28,29]. Although annealing SWNTs or DWNTs at high temperatures or applying femtosecond lasers has been shown to facilitate the production of LLCC@DWNT/SWNT, it was found that carbon chains can form between neighboring DWCNTs rather than inside the inner tubes of the DWCNTs in the heat-treatment method [30,31]. Furthermore, a key concern in this method is the source of carbon and its transformation into LLCCs: the carbon source could originate from amorphous carbon within or surrounding the CNTs or even from the CNTs themselves [31,32].

In an alternative approach, researchers have been investigating the growth of carbyne or LLCC by carefully inserting selected molecules into CNTs, acting as safe containers [33,34]. This nanoreactor method provides an excellent environment for controlling self-assembly, reactions, and the formation of metastable structures [8,34,35]. Importantly, this method requires lower temperatures for LLCC growth compared to arc-discharge and post-treatment methods, as it relies on molecular reactions rather than recrystallization of graphitic structures [8]. For example, C. Zhao et al. successfully formed LLCCs by enclosing polyyne molecules into DWCNTs and annealing them at 1000°C under high vacuum conditions [27]. Similarly, J. Zhang et al. observed Raman features related to LLCCs after heating adamantane enclosed in CNTs at temperatures ranging from 600°C to 700°C [36]. On the other hand, using such low temperatures can reduce the rate of reactions, leading to the incomplete dissociation of molecules and radicals, which may cause damage to the container [37,38]. To address this concern, an alternative option can be considered, involving the use of catalyst particles inside the tube [39,40]. In particular, our previous studies have examined the mechanism of catalytic growth of endohedral carbyne using various hydrocarbon species [37,41], along with studying the physical properties of the resulting structure [41,42]. While these investigations have provided some insights into catalytic carbyne growth, the mechanisms involved in the catalytic synthesis of carbyne from oxygen-containing hydrocarbon precursors and the specific role of oxygen in carbyne growth remain elusive. This

knowledge gap hampers a better understanding of the feedstock effect in the catalyzed growth of endohedral carbyne. Therefore, our study aims to investigate the synthesis processes of endohedral carbyne within DWNTs using a nickel catalyst and two carbon feedstocks, namely, C and CO, by employing reactive molecular dynamics (MD) simulations.

Computational details

In this study, we use the LAMMPS program [43], which is based on the reactive MD method, to simulate the carbyne synthesis processes. We employ the ReaxFF potential [44] with a parameter set developed by Zou et al. [45] to describe the interatomic interactions in the system. As a model system, we choose the $\text{Ni}_5@(\text{5,5})@(\text{10,10})$ system, which denotes that the Ni_5 nanocluster is located inside the (5,5) nanotube, which, in turn, is located inside the (10,10) nanotube. In other words, the designation ' $\text{Ni}_5@(\text{5,5})@(\text{10,10})$ ' indicates that the Ni_5 nanocluster is introduced as a catalyst particle in the (5,5)@ (10,10) DWNT (see Fig. 1). The inner and outer diameters of the DWNT are 0.68 and 1.37 nm, respectively, and these values are fairly close to the experimentally reported diameters of DWNTs; the inner diameter ranges from 0.63 to 0.79 nm, and the outer diameter ranges from 1.3 to 1.6 nm [46]. According to Shi et al. [25], the carbyne@ (5,5) configuration has the lowest interaction energy, favoring a (5,5) nanotube with a 0.69 nm diameter. The carbyne-nanotube distance is approximately 0.34 nm, similar to the graphite interlayer spacing found in experiments. Additionally, the (10,10) tube is a suitable choice as the outer tube for the (5,5) tube, as reported by Charlier et al. [47] and Saito et al. [48].

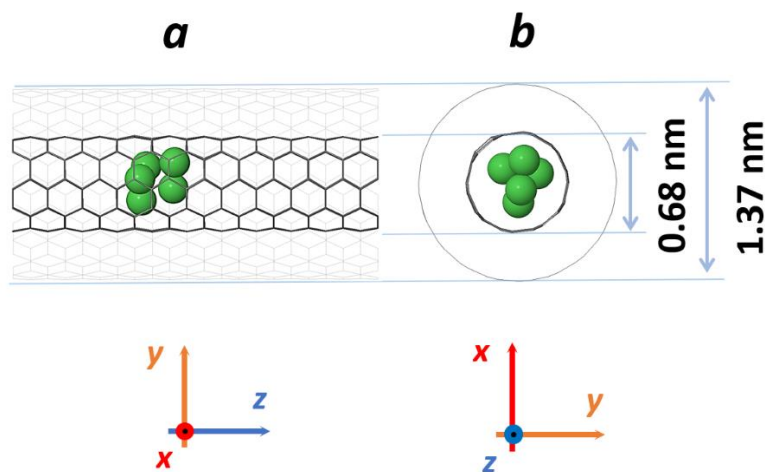


Fig. 1. Side (a) and top (b) views of the $\text{Ni}_5@(\text{5,5})@(\text{10,10})$ model system. Carbon atoms of the DWNT are not shown; light and dark gray wireframes represent the outer and inner walls of the DWNT, respectively. Ni atoms are shown as green balls.

The simulation box size is $5.0 \times 5.0 \times 2.7 \text{ nm}^3$, and periodic boundary conditions are applied in three axes. Specifically, applying them along the z-axis, which represents the length of the DWNT, allows for the simulation of an infinitely long DWNT. This suggests that the carbon chain formed inside the DWNT is theoretically infinite due to the PBC, whereas in the simulations it appears with a finite length [8]. For infinite DWNTs, estimating the filling or volume fraction of endohedral Ni atoms in the inner tube is more meaningful than using their concentration (or exact number). The volume fraction is obtained by dividing the average volume of Ni atoms by the effective volume of the inner tube of the DWNT (in %). The average volume of each Ni atom is determined using the van der Waals radius, approximately 1.63 \AA [49]. The effective volume of the inner wall of the DWNT is calculated using the concept of the effective diameter [50], represented as $d_{eff} = d_{geo} - \sigma_{C-Ni}$, where d_{eff} is the effective diameter of the inner wall of the

DWNT (0.68 nm) and σ_{C-Ni} is the sigma bond length of C–Ni (0.25 nm). According to this calculation, the inner volume fraction of the nanotube (0.39 nm^3) filled by the Ni₅ nanocluster (0.09 nm^3) is estimated to be approximately 23%, which indicates ample room for precursors and the growing chain inside the inner tube of the DWNT.

The energy of the model system is initially minimized by applying a combination of steepest descent and conjugated gradient methods. Subsequently, the temperature of the systems is increased to 1700 K (with a temperature gradient of 1 K/ps) in the NpT ensemble using a Berendsen thermostat and barostat [51]. Then, the system is equilibrated using the Bussi thermostat [52] in the NVT ensemble. Afterward, the chosen carbon precursors (i.e., C and CO) are sequentially inserted into the inner tube at an interval of 250 ps. The initial velocity of each feedstock is in a random direction, and its magnitude is set to the root-mean-square velocity, corresponding to the growth temperature (i.e., 1700 K). The impingement flux for both C and CO species is chosen to be $0.687 \text{ nm}^{-2}\text{ns}^{-1}$, and the corresponding gas pressures [53] are found to be 37.6 and 56.8 kPa, respectively. During the simulation, to keep the pressure of gas-phase molecules constant inside the DWNT, O₂ molecules are released from the system every 10^6 MD steps (i.e., 0.25 ns) [37]. A time step of 0.25 fs is used in all MD simulations, and the maximum simulation time lasts 9 ns. Normally, experimental carbyne growth takes a longer time, but a higher temperature speeds up the simulation-based growth by overcoming barriers and reducing computational costs. The simulations are conducted at least ten times for each study case, and the results are obtained by averaging the corresponding physical quantities.

Results and discussion

Fig. 2 shows the nucleation (Fig. 2, steps I-III) and continued growth (Fig. 2, steps IV and V) periods of endohedral carbyne in the presence of Ni₅ catalyst and C (a) or CO (b) precursors.

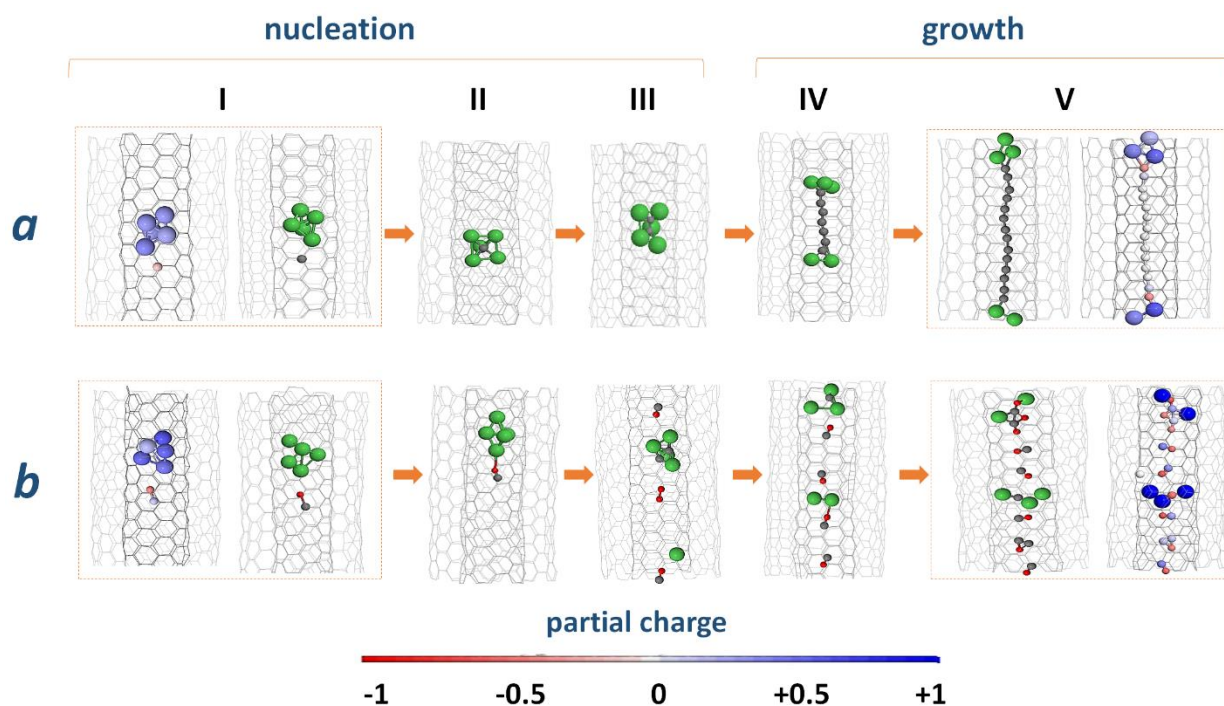


Fig. 2. Two periods of the synthesis of Ni-catalyzed endohedral carbyne in DWNT from C (a) and CO (b) radicals. Ni, C, and O atoms are depicted here in green, gray, and red colors, respectively. For clarity, the carbon atoms of DWNT are not shown. In each dashed rectangle, the same structure is shown with and without partial charges, ranging from -1 (red) to +1 (blue).

In the case of the C precursor, the carbon atom introduced into the DWNT is initially adsorbed (with an adsorption energy barrier of 0.29 eV) on the nickel cluster. Since the electronegativity of carbon atoms ($\chi_{\text{C}}=2.55$) is greater than the electronegativity of nickel atoms ($\chi_{\text{Ni}}=1.91$), the average partial charge of carbon atoms is negative ($\delta=-1.49 e$), whereas the average partial charge of nickel atoms is positive ($\delta=+1.63 e$) in the inner wall of the DWNT. As a result, the C precursor introduced into the DWNT is induced under the influence of positive nickel atoms, creates a negative partial charge ($\delta=-0.14 e$) (see Fig. 2a, step I) and attaches to the nickel cluster due to electrostatic forces (Fig. 2a, step II). Then, the C precursor diffuses on the surface of the cluster and binds with another adsorbed precursor, the calculated diffusion (0.4 eV) and binding (0.1 eV) energy barriers which correspond to reported data [41,54]. Consequently, a carbon dimer or initial carbyne nuclei appear in the DWNT (Fig. 2a, step III), and this period of synthesis (i.e., steps I-III) is called the nucleation of the carbyne structure. After the nucleation period, the nickel nanocluster splits into two smaller fragments, which bind at both ends of the carbon chain and remain throughout the entire growth period (see steps IV and V in Fig. 2a and cf. Fig. S1 in the Supporting Information). This splitting (or the structure transformation) process can be divided into four stages (see Fig. 3a).

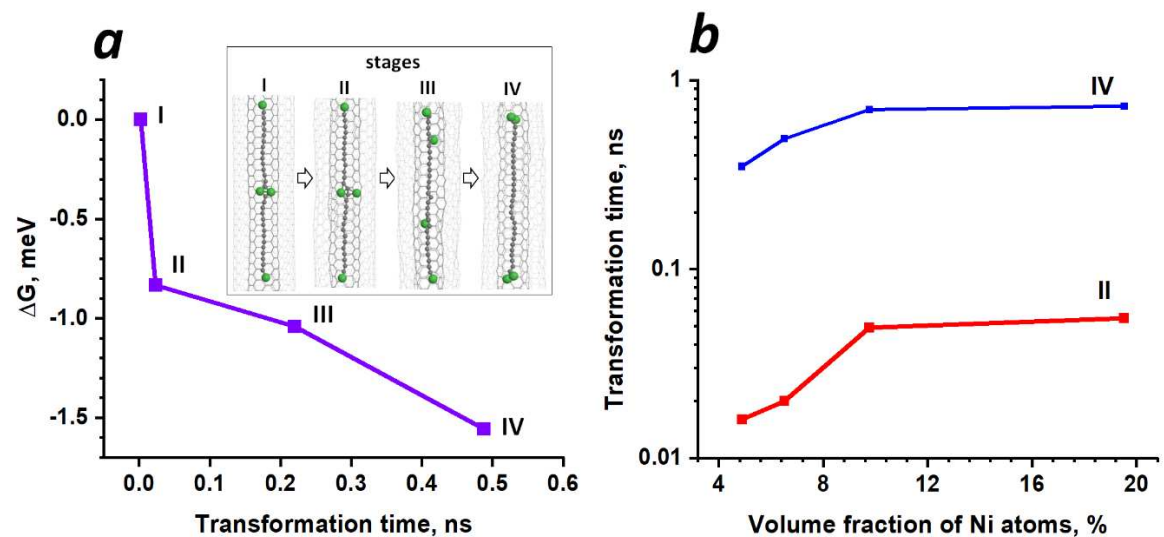


Fig. 3. (a) Transformation of the structure from $Ni_{m1}-C_{n1}-Ni_{m2}-C_{n2}-Ni_{m3}$ to $Ni_k-C_{n1+n2}-Ni_l$ in a DWNT with a volume fraction of Ni atoms of 5%. (b) Transformation times for stages II and IV as a function of the volume fraction of Ni atoms in DWNTs.

In the first stage, two separate carbon chains link through Ni atoms or nanoclusters. In the second stage, middle Ni atoms catalytically facilitate the formation of C-C bonds between these two chains, requiring an activation energy barrier of 1.5 eV. Consequently, the bonding behavior of carbon atoms prevents the stable chemical connection of nickel atoms with the central carbon atoms of the chain. As a result, weakly bonded middle nickel atoms can freely move or diffuse along the newly formed longer carbon chain during the third stage, with an activation barrier of 1.3 eV. This phenomenon is attributed to the distinct nature of carbon atom's binding in the middle and at the end of the chain. Finally, in the fourth stage, all nickel atoms connect to the terminal atoms of the chain. Throughout these stages, the energy of the thermodynamic system progressively decreases. Specifically, the molar Gibbs free energy change (ΔG) [37] is -0.83 eV, -1.04 eV, and -1.56 eV for stages II, III, and IV, respectively (see Fig. 3a). This energy decrease indicates an increase in the stability of the system during structural transformations. The results demonstrate that the second stage (binding of two separate carbon chains) and fourth stage (formation of a new longer chain with terminal nickel atoms) are fundamental in this transformation, and their duration depends on the volume fraction of nickel atoms in the DWNT (see Fig. 3b and Fig. S1). It is important to note that nickel termination at both ends of the chain prevents undesired bonding between the chain and the tube interior [17], and these nickel atoms

continuously promote the safe formation of C-C connections [41]. Our calculations show that with an increase in the length of the carbon chain per addition of one carbon atom, the energy of the chain decreases by -7.05 eV, which is in the range of values (from -5.77 eV to -7.67 eV) obtained by quantum mechanical calculations [10,14,55]. Overall, these results strongly suggest that if the growth process continues uninterrupted, an infinite carbon chain, known as carbyne [7], terminated with metal atoms, can ultimately be achieved.

In the case of the CO precursor, as in the case of the C precursor, the introduced CO radical is first adsorbed on the nickel cluster (Fig. 2b, step II) with an adsorption energy of 1.2 eV, which is very close to the experimental value of 1.1 eV [56]. The simulation results show that the radical binds to the catalyst on the oxygen side, and this phenomenon can be explained by the partial charges of the atoms of the system. As mentioned above, due to the difference in the electronegativity of carbon ($\chi_C=2.55$) and nickel ($\chi_{Ni}=1.91$) atoms, the partial charges of carbon atoms of the inner part of the DWNT turn out to be negative ($\delta=-2.03 e$), whereas the nickel atoms of the nanocluster obtain a positive charge ($\delta=+2.28 e$). On the other hand, due to the stronger electronegativity of the oxygen atom ($\chi_O=3.44$), partial charges of oxygen and carbon atoms in the CO radical become $\delta=-0.40 e$ and $\delta=+0.15 e$ (Fig. 2b, step I). As a result, CO binds to the catalyst on its oxygen side because of the electrostatic interactions between the positive nickel and negative oxygen atoms. Then, CO radicals diffuse (with a diffusion energy barrier of 0.2 eV) on the surface of the catalyst, followed by the dissociation of the C-O bond (with a dissociation energy barrier of 2.5 eV) caused by the nickel catalyst, which reduces the dissociation energy barrier of the bond by approximately 3.6 times. As a continuation, a newly dissociated carbon atom binds (with a binding energy barrier of 0.1 eV) to a previously dissociated carbon atom and consequently forms a carbon dimer (Fig. 2b, step III). This process corresponds to the nucleation period of the catalyzed carbyne growth from the CO precursor. Simultaneously, the remaining oxygen atoms either bind each other (with a binding energy of 5.4 eV) and leave the nanocluster surface as O₂ molecules or form a strong Ni-O bond (with a binding energy of 3.9 eV) as a result of breaking the Ni-Ni bond (with a dissociation energy of 2.4 eV).

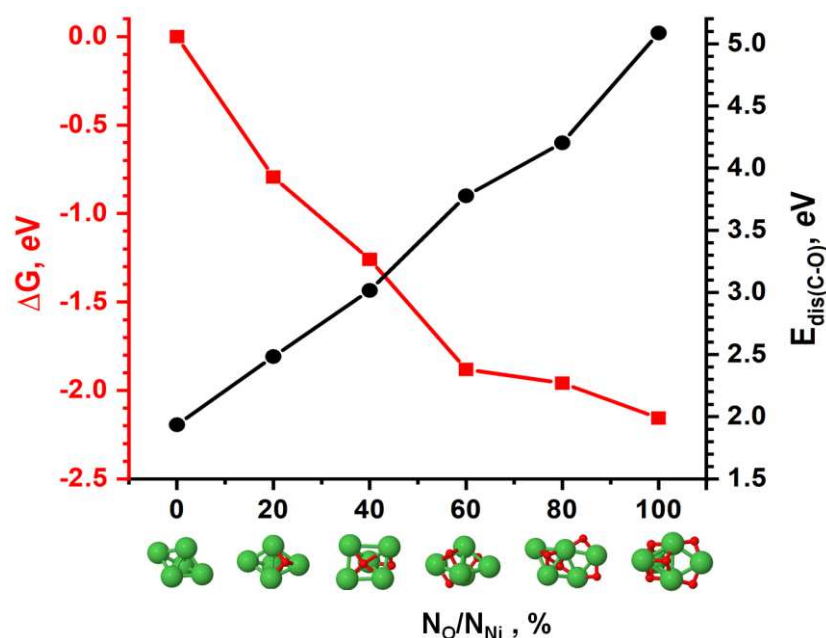


Fig. 4. Molar Gibbs free energy of the nanocatalyst (red) and the dissociation energy of the C-O bond (black) as a function of the oxidation state of the nanocatalyst.

In the continued growth period (Fig. 2b, steps IV and V), as a result of the gradual breaking of Ni-Ni bonds and the formation of Ni-O bonds, the nanocatalyst is rapidly oxidized, and the change of molar Gibbs free energy [37] of the resulting Ni_xO_y nanocluster decreases constantly

(Fig. 4). In particular, the molar Gibbs free energy changes from 0 to -2.2 eV when the oxidation state of the cluster is changed from 0 to 100 %, thereby indicating the formation of a stable nanocatalyst. Consequently, the oxidation of nanocatalysts leads to a loss of their catalytic properties or poisoning. When the catalyst is completely oxidized, the energy required for the dissociation of C-O bonds on the catalyst surface increases by 2.5 times (Fig. 4, black curve). According to the theory of active centers [57], in the process of catalyst poisoning, the poison (i.e., oxygen atoms) is strongly adsorbed on the active sites of the catalyst and covers it. Due to the formation of strong chemical bonds between the poison and the active sites of the catalyst, it becomes very difficult for reagents (CO) to displace the poison and move to the active centers. As a consequence, the catalyst loses its catalytic properties and causes CO radicals to remain in the gas environment without decomposing. This, in turn, leads to the interruption of the carbon supply and consequently the growth of carbyne.

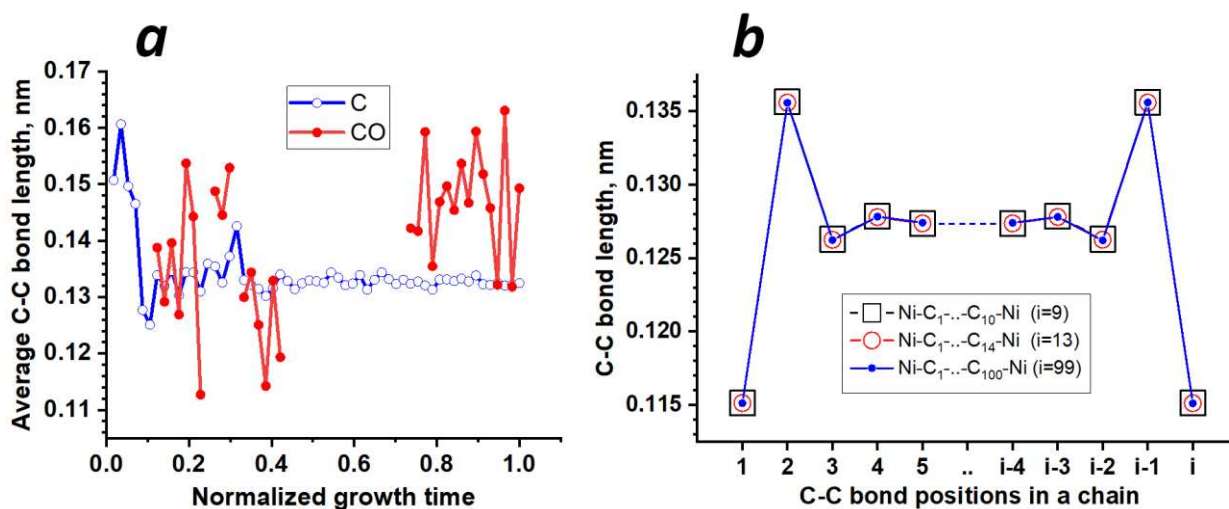


Fig. 5. (a) Evolution of the C-C bond length in grown carbon chains as a function of the normalized growth time. (b) Bond length alternation in the nickel-terminated carbyne consisting of 10, 14 and 100 C atoms.

In addition to studying the growth mechanism dependent on the feedstock, it is also important to assess the growth kinetics and analyze the structure. Figure 5a shows that the average C-C bond length in the grown chain initially fluctuates significantly (ranging from 0.125 nm to 0.16 nm) during the growth of the C feedstock cases (see Fig. 5a, C). However, it eventually stabilizes at approximately 0.132 nm (cf. Fig. 2a, V), which closely matches experimental measurements for the C-C bond length (i.e., 0.131 nm) in a metalated carbyne [21]. Carbyne typically prefers a polyynes structure (...-C≡C-C≡C-...) with alternating C-C bond lengths due to the Peierls distortion [58]. At absolute zero temperature, the obtained Ni-C₁-...-C₁₄-Ni structure (cf. Fig. 2a, V) exhibits an average bond length alternation (BLA=|r₁-r₂|) of approximately 6.71 pm (Fig. 5b, red open circles). In particular, the BLA changes from 20.59 pm (near the chain end) to 0.23 pm (in the inner part of the chain), indicating a combination of polyynes and cumulene-like (...=C=C=C=C=...) characteristics along the chain [55,59]. Such a similar character is also observed in the cases of the nickel-terminated carbyne structure with 10 and 100 C atoms (see Fig. 5b, black open squares and blue dots, respectively). Although the chain structure has this dual character, most parts of the chain display a cumulene-like structure with an average bond length of 0.1275 nm, consistent with the stable cumulene structure (with a length of 0.1282 nm) obtained from *ab initio* calculations for the inner part of the chain containing more than 10 atoms [55]. Furthermore, other DFT calculations show an energy difference of 2 meV per carbon between polyynes and cumulene structures [10]. Consequently, the carbyne structure transforms from polyynes to cumulene-like due to zero-point atomic vibrations, resulting in the stability of the latter carbyne structure [4].

In contrast to the C feedstock cases, where we observe a well-defined chain structure with polyyne-cumulene character, the CO feedstock case shows completely different behavior. Instead of a continuous and ordered chain, the CO feedstock leads to the appearance of only a few C-C bonds with varying lengths ranging from 0.112 nm to 0.164 nm (see Fig. 5a, CO). This indicates a more complex and irregular arrangement of carbon atoms, making it challenging to assign a specific chain with a polyyne-cumulene character in this case.

Conclusions

Using reactive molecular dynamics (MD) simulations, we investigated the growth mechanisms of encapsulated carbyne in double-walled carbon nanotubes (DWNT) catalyzed by nickel (Ni) from carbon (C) and carbon monoxide (CO) feedstocks. Our results revealed that the presence of a Ni cluster facilitates the formation of long carbyne chains when C precursors are introduced into the DWNT. In contrast, the insertion of CO radicals into the tube leads to the oxidation of the Ni cluster due to radical dissociation. Consequently, the catalytic activity of the Ni catalyst diminishes gradually, eventually resulting in its poisoning. Unlike C precursors, CO radicals solely contribute to the formation of carbyne nuclei, where subsequently introduced radicals remain in the gas phase without decomposition, leading to the cessation of carbyne chain growth. This study enhances our understanding of the synthesis mechanisms of long carbyne structures by considering the catalyst-feedstock tandem.

Supplementary Material

Transformation steps of the structure from $\text{Ni}_{m1}\text{-C}_{n1}\text{-Ni}_{m2}\text{-C}_{n2}\text{-Ni}_{m3}$ to $\text{Ni}_k\text{-C}_{n1+n2}\text{-Ni}_l$ in double-walled carbon nanotubes with different volume fractions of endohedral nickel atoms.

Acknowledgment

The authors gratefully acknowledge the financial support from the Agency for Innovative Development of the Republic of Uzbekistan, grant number F-FA-2021-512. Simulations were carried out using the supercomputer cluster of the Institute of Ion-Plasma and Laser Technologies of the Academy of Sciences of Uzbekistan.

References

- [1] V. Meunier et al., *Carbon science perspective in 2022: Current research and future challenges*. Carbon **195**, 272 (2022).
- [2] A. M. Sladkov & Y. P. Kudryavtsev, *Polyynes*. Russian Chemical Reviews **32**, 229 (1963).
- [3] R. J. Lagow et al., *Synthesis of Linear Acetylenic Carbon: The “Sp” Carbon Allotrope*, Science **267**, 362 (1995).
- [4] V. I. Artyukhov, M. Liu & B. I. Yakobson, *Mechanically induced metal–insulator transition in carbyne*. Nano Letters **14**, 4224 (2014).
- [5] Y. Gao & R. R. Tykwinski, *Advances in polyynes to model carbyne*. Accounts of Chemical Research **55**, 3616 (2022).
- [6] A. Bianco et al., *A carbon science perspective in 2018: Current achievements and future challenges*. Carbon **132**, 785 (2018).
- [7] C. S. Casari et al., *Carbon-atom wires: 1-D systems with tunable properties*. Nanoscale **8**, 4414 (2016).

- [8] K. Zhang, Y. Zhang & L. Shi, *A review of linear carbon chains*. Chinese Chemical Letters **31**, 1746 (2020).
- [9] C. S. Casari & A. Milani, *Carbyne: from the elusive allotrope to stable carbon atom wires*. MRS Communications **8**, 207 (2018).
- [10] M. Liu, V. I. Artyukhov, H. Lee, F. Xu, and B. I. Yakobson, *Carbyne from First Principles: Chain of C Atoms, a Nanorod or a Nanorope*, ACS Nano **7**, 10075 (2013).
- [11] M. Wang and S. Lin, *Ballistic Thermal Transport in Carbyne and Cumulene with Micron-Scale Spectral Acoustic Phonon Mean Free Path*, Sci Rep **5**, 18122 (2015).
- [12] Y. Prazdnikov, *Prospects of Carbyne Applications in Microelectronics*, Journal of Modern Physics **02**, (2010).
- [13] P. B. Sorokin et al., *Calcium-decorated carbyne networks as hydrogen storage media*. Nano Letters **11**, 2660 (2011).
- [14] B. Pan, J. Xiao, J. Li, P. Liu, C. Wang, and G. Yang, *Carbyne with Finite Length: The One-Dimensional sp Carbon*, Science Advances **1**, e1500857 (2015).
- [15] D. W. Boukhvalov, I. S. Zhidkov, E. Z. Kurmaev, E. Fazio, S. O. Cholakh, and L. D'Urso, *Atomic and Electronic Structures of Stable Linear Carbon Chains on Ag-Nanoparticles*, Carbon **128**, 296 (2018).
- [16] X. Zhao, Y. Ando, Y. Liu, M. Jinno, and T. Suzuki, *Carbon Nanowire Made of a Long Linear Carbon Chain Inserted Inside a Multiwalled Carbon Nanotube*, Phys. Rev. Lett. **90**, 187401 (2003).
- [17] W. Q. Neves et al., *Effects of Pressure on the Structural and Electronic Properties of Linear Carbon Chains Encapsulated in Double Wall Carbon Nanotubes*, Carbon **133**, 446 (2018).
- [18] N. F. Andrade, T. L. Vasconcelos, C. P. Gouvea, B. S. Archanjo, C. A. Achete, Y. A. Kim, M. Endo, C. Fantini, M. S. Dresselhaus, and A. G. Souza Filho, *Linear Carbon Chains Encapsulated in Multiwall Carbon Nanotubes: Resonance Raman Spectroscopy and Transmission Electron Microscopy Studies*, Carbon **90**, 172 (2015).
- [19] M. Kijima, Y. Sakai, and H. Shirakawa, *Electrochemical Synthesis of Carbyne Catalyzed by Nickel Complex*, Synthetic Metals **71**, 1837 (1995).
- [20] E. Kano, M. Takeguchi, J. Fujita, and A. Hashimoto, *Direct Observation of Pt-Terminating Carbyne on Graphene*, Carbon **80**, 382 (2014).
- [21] Q. Sun et al., *Bottom-Up Synthesis of Metalated Carbyne*, J. Am. Chem. Soc. **138**, 1106 (2016).
- [22] C. Jin, H. Lan, L. Peng, K. Suenaga, and S. Iijima, *Deriving Carbon Atomic Chains from Graphene*, Phys. Rev. Lett. **102**, 205501 (2009).
- [23] V. Scuderi, S. Scalese, S. Bagiante, G. Compagnini, L. D'Urso, and V. Privitera, *Direct Observation of the Formation of Linear C Chain/Carbon Nanotube Hybrid Systems*, Carbon **47**, 2134 (2009).
- [24] C. S. Casari et al., *Low-frequency modes in the Raman spectrum of sp² nanostructured carbon*. Physical Review B **77**, 195444 (2008).
- [25] L. Shi et al., *Confined Linear Carbon Chains as a Route to Bulk Carbyne*, Nature Mater **15**, 6 (2016).
- [26] S. Toma, K. Asaka, M. Irita, and Y. Saito, *Bulk Synthesis of Linear Carbon Chains Confined inside Single-Wall Carbon Nanotubes by Vacuum Discharge*, SURF INTERFACE ANAL **51**, 131 (2019).
- [27] C. Zhao, R. Kitaura, H. Hara, S. Irlle, and H. Shinohara, *Growth of Linear Carbon Chains inside Thin Double-Wall Carbon Nanotubes*, J. Phys. Chem. C **115**, 13166 (2011).
- [28] S. Heeg et al., *Carbon nanotube chirality determines properties of encapsulated linear carbon chain*. Nano Letters **18**, 5426 (2018).
- [29] L. Shi et al., *Toward confined carbyne with tailored properties*. Nano Letters **21**, 1096 (2021).
- [30] M. Endo et al., *Nanotube Coalescence-Inducing Mode: A Novel Vibrational Mode in Carbon Systems*. Small **2**, 1031 (2006).

- [31] J. Ha et al., *Ultrafast structural evolution and formation of linear carbon chains in single-walled carbon nanotube networks by femtosecond laser irradiation*. *Nanoscale* **9**, 16627 (2017).
- [32] L. Shi et al., *Templated direct growth of ultra-thin double-walled carbon nanotubes*. *Nanoscale* **10**, 21254 (2018).
- [33] P. M. Ajayan & S. Iijima, *Capillarity-induced filling of carbon nanotubes*. *Nature* **361**, 333 (1993).
- [34] A. N. Khlobystov, D. A. Britz & G. A. D. Briggs, *Molecules in carbon nanotubes*. *Accounts of Chemical Research* **38**, 901 (2005).
- [35] H. Shinohara, *Peapods: Exploring the inner space of carbon nanotubes*. *Japanese Journal of Applied Physics* **57**, 020101 (2017).
- [36] J. Zhang et al., *Synthesis and transformation of linear adamantane assemblies inside carbon nanotubes*. *ACS Nano* **6**, 8674 (2012).
- [37] U. Khalilov and E. C. Neyts, *Mechanisms of Selective Nanocarbon Synthesis inside Carbon Nanotubes*, *Carbon* **171**, 72 (2021).
- [38] U. Khalilov et al., *Nanoscale mechanisms of CNT growth and etching in plasma environment*. *Journal of Physics D: Applied Physics* **50**, 184001 (2017).
- [39] X. Pan & X. Bao, *The effects of confinement inside carbon nanotubes on catalysis*. *Accounts of Chemical Research* **44**, 553 (2011).
- [40] S. A. Miners, G. A. Rance, & A. N. Khlobystov, *Chemical reactions confined within carbon nanotubes*. *Chemical Society Reviews* **45**, 4727 (2016).
- [41] U. Khalilov, C. Vets, and E. C. Neyts, *Catalyzed Growth of Encapsulated Carbyne*, *Carbon* **153**, 1 (2019).
- [42] G. R. Berdiyrov, U. Khalilov, H. Hamoudi & E. Neyts, *Effect of chemical modification on electronic transport properties of carbyne*. *Journal of Computational Electronics* **20**, 848 (2021).
- [43] A. P. Thompson et al., *LAMMPS - a Flexible Simulation Tool for Particle-Based Materials Modeling at the Atomic, Meso, and Continuum Scales*, *Computer Physics Communications* **271**, 108171 (2022).
- [44] A. C. T. van Duin, S. Dasgupta, F. Lorant, and W. A. Goddard, *ReaxFF: A Reactive Force Field for Hydrocarbons*, *J. Phys. Chem. A* **105**, 9396 (2001).
- [45] C. Zou, Y. K. Shin, A. C. T. van Duin, H. Fang, and Z.-K. Liu, *Molecular Dynamics Simulations of the Effects of Vacancies on Nickel Self-Diffusion, Oxygen Diffusion and Oxidation Initiation in Nickel, Using the ReaxFF Reactive Force Field*, *Acta Materialia* **83**, 102 (2015).
- [46] G. Chen, S. Bandow, E. Margine, C. Nisoli, A. Kolmogorov, V. Crespi, R. Gupta, G. Sumanasekera, S. Iijima, and P. Eklund, *Chemically Doped Double-Walled Carbon Nanotubes: Cylindrical Molecular Capacitors*, *Physical Review Letters* **90**, 257403 (2003).
- [47] A. Charlier, E. McRae, R. Heyd, M. F. Charlier & D. Moretti, *Classification for double-walled carbon nanotubes*, *Carbon* **37**, 1779, (1999)
- [48] R. Saito, G. Dresselhaus & M.S. Dresselhaus, *Electronic structure of double-layer graphene tubules*, *Journal of Applied Physics* **73**, 494 (1993).
- [49] A.V. Bondi, *Van der Waals volumes and radii*, *The Journal of Physical Chemistry* **68**, 441 (1964).
- [50] A. Peigney et al., *Specific Surface Area of Carbon Nanotubes and Bundles of Carbon Nanotubes*, *Carbon* **39**, 507 (2001).
- [51] H. Berendsen, J. P. M. Postma, W. van Gunsteren, A. DiNola, and J. R. Haak, *Molecular-Dynamics with Coupling to An External Bath*, *The Journal of Chemical Physics* **81**, 3684 (1984).
- [52] G. Bussi, D. Donadio, and M. Parrinello, *Canonical Sampling Through Velocity Rescaling*, *The Journal of Chemical Physics* **126**, 014101 (2007).

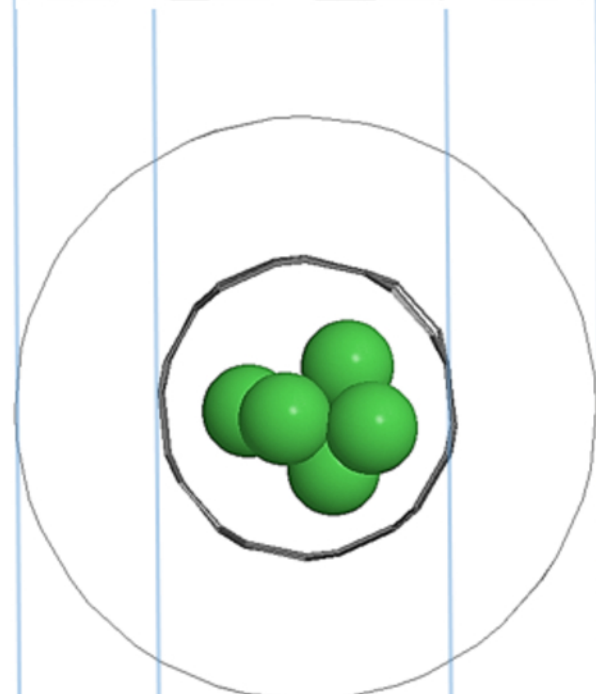
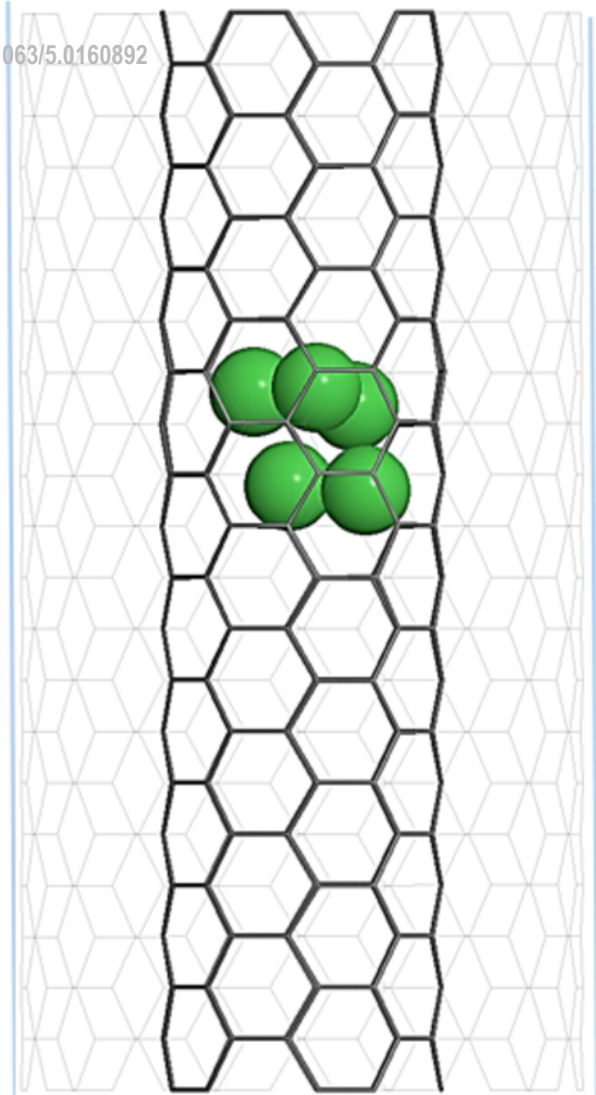
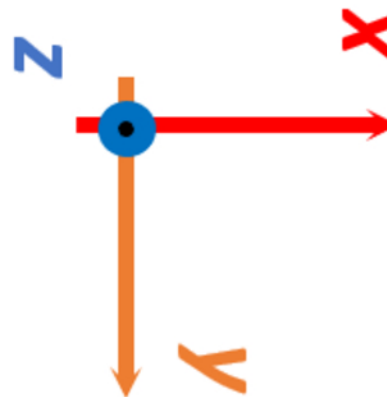
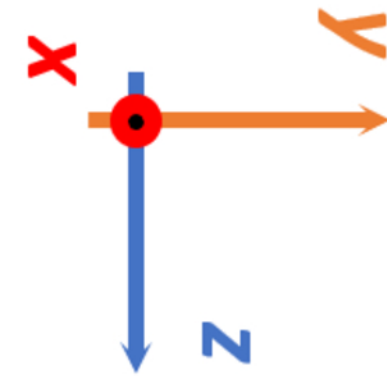
This is the author's peer reviewed, accepted manuscript. However, the online version of record will be different from this version once it has been copyedited and typeset.

PLEASE CITE THIS ARTICLE AS DOI: 10.1063/1.50160892

- [53] U. Khalilov, A. Bogaerts, and E. C. Neyts, *Microscopic Mechanisms of Vertical Graphene and Carbon Nanotube Cap Nucleation from Hydrocarbon Growth Precursors*, *Nanoscale* **6**, 9206 (2014).
- [54] Y.-H. Shin and S. Hong, *Carbon Diffusion around the Edge Region of Nickel Nanoparticles*, *Appl. Phys. Lett.* **92**, 043103 (2008).
- [55] A. Timoshevskii, S. Kotrechko, and Yu. Matviychuk, *Atomic Structure and Mechanical Properties of Carbyne*, *Phys. Rev. B* **91**, 245434 (2015).
- [56] H. H. Madden, J. Küppers, and G. Ertl, *Interaction of Carbon Monoxide with (110) Nickel Surfaces*, *J. Chem. Phys.* **58**, 3401 (1973).
- [57] A. Bahl, *Essentials of Physical Chemistry*, edition 28, (S Chand Publishing, New Delhi, 2019).
- [58] Peierls, R.E. Quantum theory of solids. Oxford University Press (1955).
- [59] X. Fan, L. Liu, J. Lin, Z. Shen & J. L. Kuo, *Density functional theory study of finite carbon chains*. *ACS Nano* **3**, 3788 (2009).

This is the author's peer reviewed, accepted manuscript. However, the online version of record will be different from this version once it has been copyedited and typeset.

PLEASE CITE THIS ARTICLE AS DOI: 10.1063/5.0160892



0.68 nm



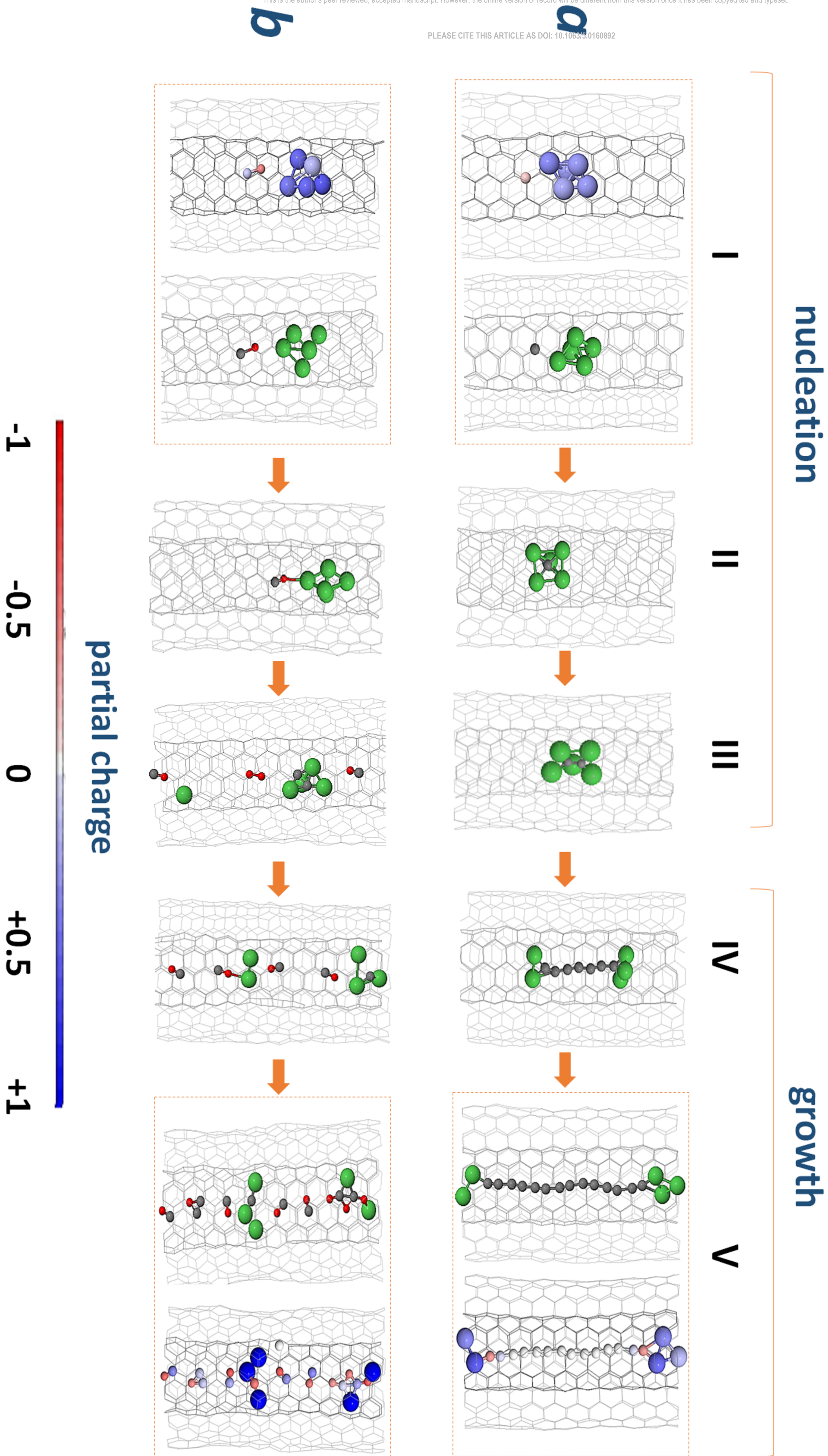
1.37 nm

a

b

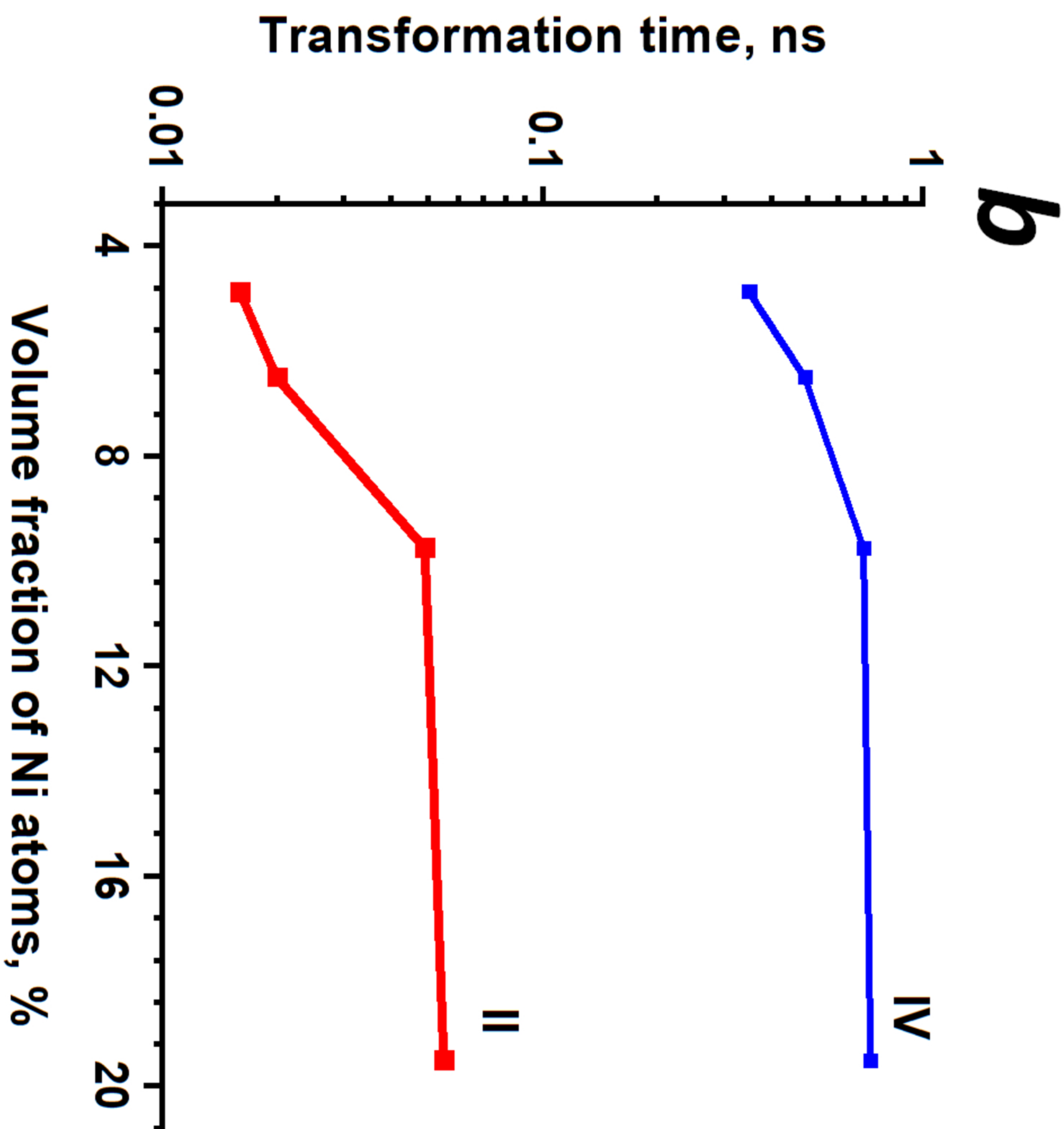
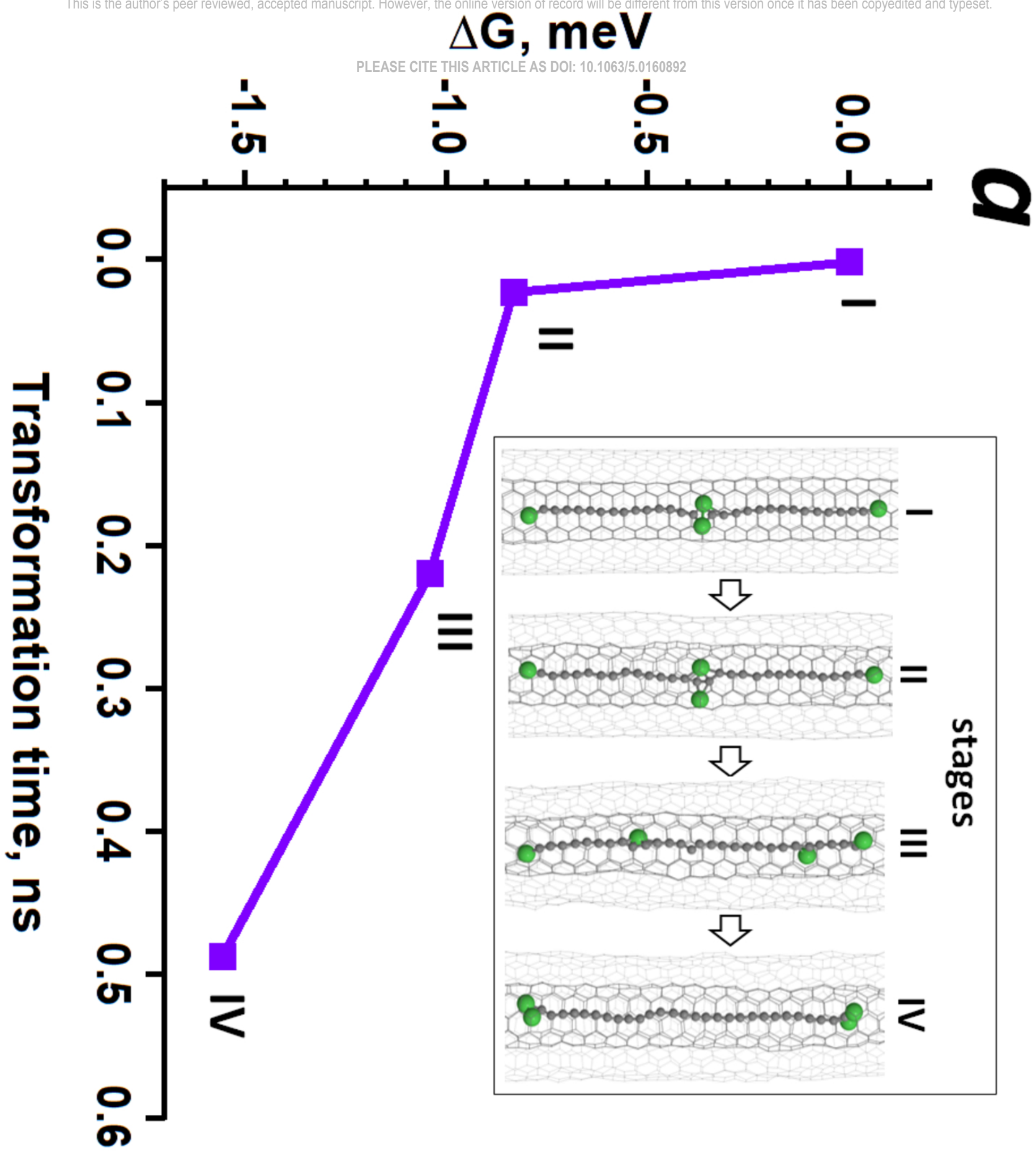
This is the author's peer reviewed, accepted manuscript. However, the online version of record will be different from this version once it has been copyedited and typeset.

PLEASE CITE THIS ARTICLE AS DOI: 10.1063/1.5160892

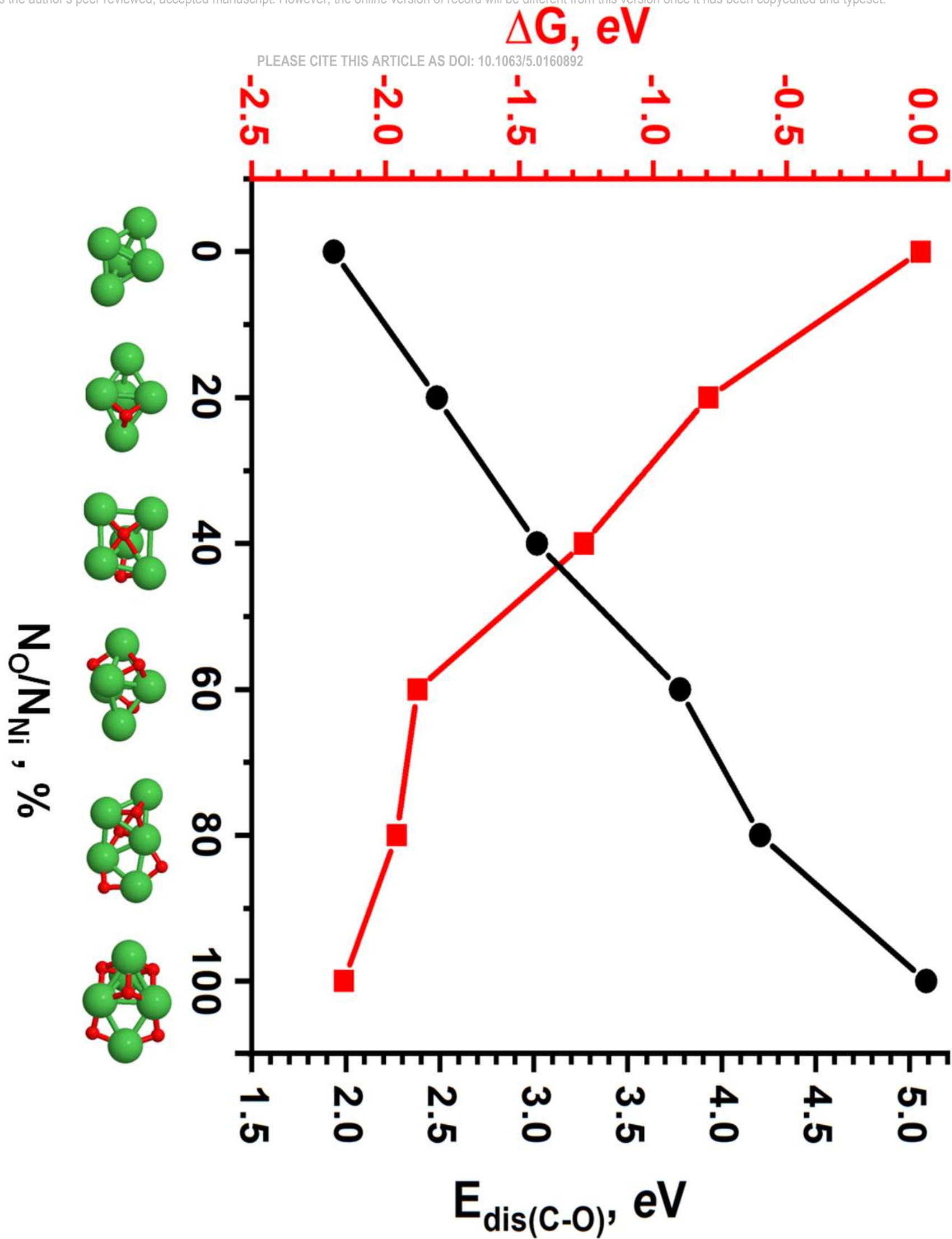


This is the author's peer reviewed, accepted manuscript. However, the online version of record will be different from this version once it has been copyedited and typeset.

PLEASE CITE THIS ARTICLE AS DOI: 10.1063/5.0160892



This is the author's peer reviewed, accepted manuscript. However, the online version of record will be different from this version once it has been copyedited and typeset.



This is the author's peer reviewed, accepted manuscript. However, the online version of record will be different from this version once it has been copyedited and typeset.

